RSC Publishing Faraday Discussions

Quantum Interferences Among Dexter Energy Transfer Pathways

Journal:	*Faraday Discussions*
Manuscript ID	FD-ART-01-2019-000007
Article Type:	Paper
Date Submitted by the Author:	14-Jan-2019

Complete List of Authors:	Bai, Shuming; Duke University Zhang, Peng; Duke University, Chemistry Antoniou, Panayiotis ; Univeristy of Cyprus, Physics Skourtis, Spiros; Univeristy of Cyprus, Physics Beratan, David; Duke University, Department of Chemistry

Quantum Interferences Among Dexter Energy Transfer Pathways

Shuming Bai[1], Peng Zhang[1], Panos Antoniou[2], Spiros S. Skourtis[2], and David N. Beratan[1,3,4]

[1]Departments of Chemistry, Duke University, Durham, NC 27708

[2]Department of Physics, University of Cyprus, Nicosia, Cyprus

[3]Department of Biochemistry, Duke University, Durham, NC 27710

[4]Department of Physics, Duke University, Durham, NC 27708

Abstract

Dexter energy transfer in chemical systems moves an exciton (i.e., an electron – hole pair) from a donor chromophore to an acceptor chromophore through a bridge by a combination of bonded and non-bonded interactions, the latter mediated by the coulomb operator. The transition is enabled by both one-electron/one-particle and two-electron/two-particle interaction mechanisms. Assuming that there is no real intermediate state population of an electron, hole, or exciton in the bridge, the transport involves two states that are non-adiabatically coupled. As such, coherent quantum interferences arise among the Dexter energy coupling pathways. These interferences, while related to those well understood interferences in single electron transfer, are much richer because of their two particle nature, since the transfer of a triplet exciton involves the net transfer of an electron and a hole. Despite this additional complexity, simple rules can govern Dexter coupling pathway interferences in special cases. As in the case of single-electron transfer, identical parallel coupling pathways can be constructively interfering and may enhance the Dexter transfer rate. Because of the virtual particle combinatorics associated with two-particle superexchange, parallel Dexter coupling routes could be expected to enhance Dexter couplings by more than a factor of two. We explore Dexter coupling pathway interferences in non-covalent assemblies, employing a method that enables the assessment of Dexter coupling pathway strengths, interferences, and origins in the context of one-particle and two-particle (i.e., coulombic) operators.

1. Introduction

> "Any other situation in quantum mechanics, it turns out, can always be explained by saying, 'You remember the case of the experiment with two holes? It's the same thing.' "
> -- R.P. Feynman, *The Character of Physical Law*, 1965, p. 130.

The directed flow of electronic excitation energy through molecules and their assemblies is essential for the efficient capture and conversion of solar energy in living and man-made structures.[1, 2] Excitation energy transport to a photocatalytic site, or to an interface that generates free carriers, allows solar energy to be stored in forms that are less ephemeral than electronic excited states. The mechanism of electronic excitation energy transfer depends on the spin states of the associated chromophores. When the energy donor and acceptor species have different spins, the process occurs by the so-called Dexter mechanism. The Dexter coupling originates in the exchange interaction between donor and acceptor and, as such, is mediated by through-bond and through-space coupling. This contrasts to the case of dipole-dipole coupling for the more familiar case of spin-allowed Förster energy transfer.[2, 3]

Here, we explore the mechanism of bridge-mediated Dexter energy transfer between chromophores that change spin states during the energy transfer reaction. Triplet energy transfer is the most familiar example of a Dexter excitation energy process, i.e., $[^3D^* \ ^1A] \rightarrow [^1D \ ^3A^*]$. Here, D and A represent the energy donor and acceptor species, respectively. Dexter transfer may appear to be spin forbidden, since both D and A undergo a spin change, but it is not. The *overall* spin is conserved, and the reaction is formally allowed. While Dexter energy transfer reactions are ubiquitous, the molecular features that control the DA coupling, and thus the energy transfer kinetics, are poorly understood. The changes in D and A local spin states cause Dexter transfer to be electric-dipole forbidden, disabling the Förster mechanism that underpins fluorescence resonant energy transfer (FRET), a workhorse mechanism used as a "molecular ruler" at the nanoscale. Strategies to control Dexter energy transfer rates are poorly developed in comparison with Förster mechanisms, despite the fact that Deter mechanism are potentially much richer in their molecular structure dependence. Figure 1 summarizes some of the energy capture and conversion structures that rely on Dexter-mechanism energy transfer.

Here, we develop a framework to explore the strength and quantum mechanical interferences among Dexter coupling pathways. The bridge-mediated Dexter coupling problem is very similar to that of bridge-mediated electron transfer.[4] With Dexter energy transfer, however, the landscape

is further complicated by the transit of two particles between donor and acceptor.

The theoretical methods used here, and the molecular insights thus derived, may prove useful in the design and interpretation of light harvesting structures, as well as for developing phosphorescence resonant energy transfer probes of distance and structure at the nanoscale.

1.1 Dexter Energy Transfer

In weak donor-acceptor electronic coupling regime, the initial and final (diabatic) states are well localized, and the anti-symmetrized approximate initial (D*A) and final (DA*) states are indicated in eq. 1.[4] The operator $V = 1/r_{12}$ couples these states and enables energy transfer. The first term in Eq. 2, through a multipole expansion, produces the Förster interaction (non-zero when D and D* have the same spin, and A and A* have the same spin).[5]

$$\Psi_I = \frac{1}{\sqrt{2}}\left[D^*(1)A(2) - D^*(2)A(1)\right] \quad (1a)$$

$$\Psi_F = \frac{1}{\sqrt{2}}\left[D(1)A^*(2) - D(2)A^*(1)\right] \quad (1b)$$

$$\langle \Psi_I \,|\, V \,|\, \Psi_F \rangle \approx \langle D^*(1)D(1) \,|\, V \,|\, A(2)A^*(2) \rangle - \langle D^*(1)A^*(1) \,|\, V \,|\, D(2)A(2) \rangle \quad (2)$$

Förster interactions decay with the inverse cube of the DA distance, while the Dexter (exchange) term has an approximately exponential distance dependence.[6] Since Dexter's pioneering analysis of this problem in 1953, it was found that the second-order application of the one-electron interaction operator also couples D*A and DA* states, also with an approximately exponential distance dependence.

When D* and A are linked chemically, the Dexter coupling is expected to be enhanced as the barrier for neutral and charge-transfer exciton propagation through the bridge is lowered. Dexter transfer is mediated by both virtual exciton states of the bridge (both electron and hole on bridge) and by charge-transfer states (just one virtual particle on the bridge). Interestingly, these states can be created by the $1/r_{12}$ operator or by repeated action of the one-electron Hamiltonian operator. We will explore both sources of DA couplings, coupling pathway mechanisms, and coupling pathway interferences.

1.2 Dexter energy transfer in energy science.

Many natural and synthetic light-harvesting structures employ Dexter energy transfer. Synthetic solar energy harvesting and concentrating schemes based on transition metals (e.g., ruthenium and osmium),[7, 8] lanthanides,[9] quantum dots (e.g., PbSe and CdSe),[10-12] organic and organometallic polymers, molecule-nanoparticle junctions, and metal-organic framework materials (MOFs)[13, 14] employ Dexter energy transfer (see Figure 1). In biology, Dexter energy transfer degrades potentially destructive triplet excited states that can produce oxidative damage if they are not deactivated.[15] Dexter energy transfer also enables electronic excitation energy up-conversion in some systems, a process that creates high energy electronic excited states from multiple lower-energy excitons.[16]

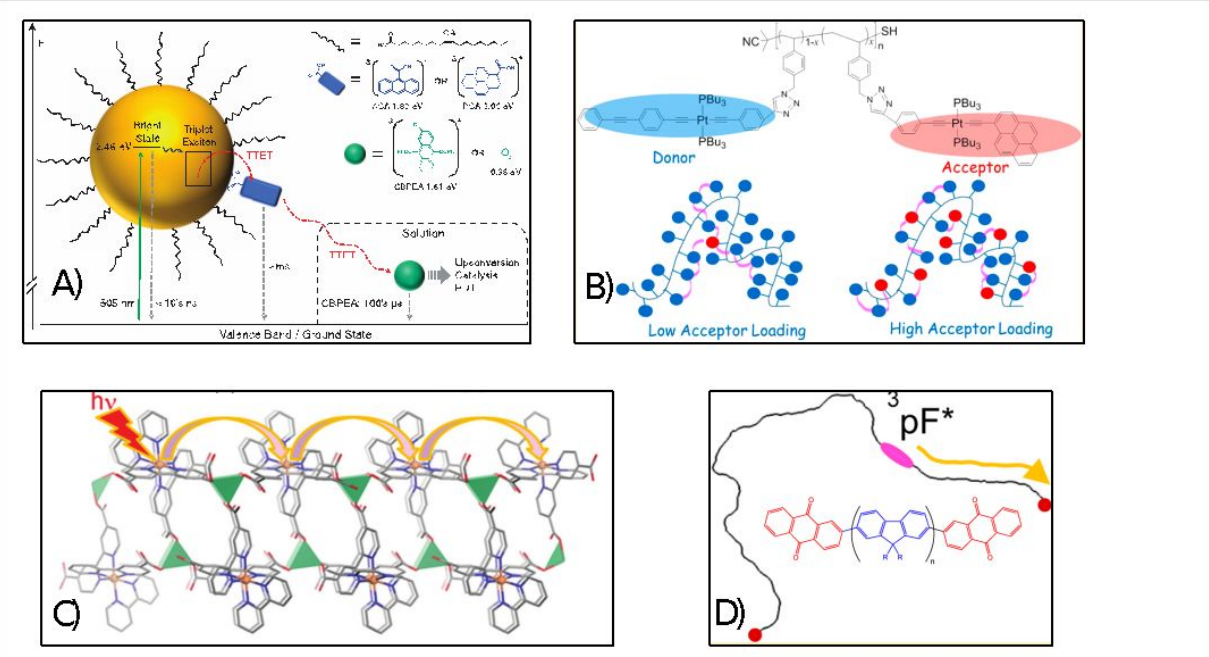

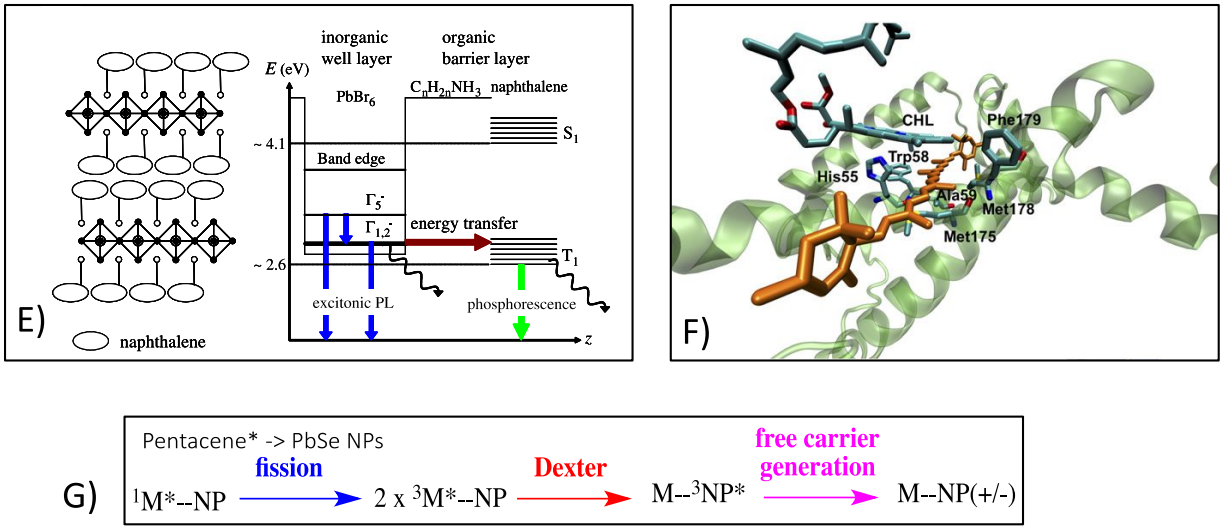

Figure 1. Examples of Dexter mechanism energy transfer reactions in key energy capture and conversion structures. (A) triplet-triplet energy transfer reactions between a nanoparticle (NP) and organic chromophores at the NP surface and with a second acceptor species in solution. (B) exciton migration and trapping in -polymer networks consisting or Pt chromophores;[17] (C) multi-step exciton hopping among Ru chromophores in a metal-organic framework structure with lightly doped Os exciton traps;[13] (D) triplet exciton hopping over 100 nm along a *single* organic polymer chain, consisting of organic fluorene chromophores with traps at chain termini;[18] (E) Wannier to Frenkel exciton conversion in perovskites via Dexter energy transfer between high spin $PbBr_6$ donors and naphthalene-derivative acceptors;[19] (F) the leutine 2 (conjugated structure, drawn in orange), binds to the light harvesting complex II (LHCII) and quenches triplet Chl excited states via Dexter energy transfer, serving a photo-protectant;[20] (G) Dexter energy transfer enables the injection of triplet excitons from small molecules to nanoparticles following exciton fission. Transport in the nanoparticle itself involves Dexter transfer, finally leading to free carrier generation.[12] Figure adapted from cited references.

Coupling pathway analysis based on Green's function methods and the CIS formalism were used recently to explore the contributions of bridge exciton and charge-transfer virtual states on Dexter transfer.[3] These studies found that the triplet-triplet donor-acceptor exciton coupling contains contributions from bridge exciton intermediates that had been ignored in previous theories (*vide infra*). These virtual intermediate states have both electron and hole on the bridge. It was found that virtual states of this kind may provide most of the triplet-triplet coupling for long bridges or bridges with energetically low-lying excited states. The bridge excitons may contribute both to pathways mediated by the one-electron component of the Hamiltonian or the coulombic two-

electron component of the Hamiltonian. Ref.[21] describes simple analytical models for bridge exciton pathways of this kind, allowing the study of quantum interferences among Dexter coupling pathways.

1.3 Dexter pathway, electron transfer pathways, and quantum interference.

Dexter transport is mediated by both bridge virtual exciton states ($B^{+/-}$ = $B_1^{+/-}B_2$, $B_1B_2^{+/-}$, $B_1^{+}B_2^{-}$ or $B_1^{-}B_2^{+}$ states in a two-unit bridge) *and* charge-transfer exciton states ($D^{+}B^{-}A$, $D^{-}B^{+}A$, $D^{+}BA^{-}$, etc.). Figures 2 and 3 show schematic representations of virtual states and Dexter coupling pathways for DBA structures. We found that when B→B*, D→D* and A→A* transition energies are close in energy, virtual bridge excitons contribute strongly to the Dexter coupling. $D^{+}A^{-}$, charge transfer excitons dominate when the B→B* transition energies are of much higher energy than the D→D* and A→A* excitation energies. However, there is a competition between the energy cost required to accomplish electron-hole separation (disfavoring the formation of CT states) and the energy cost to inject both the electron and the hole to the bridge (disfavoring the formation of the B* state).

An early model of Closs, Miller, Piotrowiak, Johnson, MacInnis, and Fleming described the Dexter coupling as a product of electron and hole superexchange interactions, valid when: (1) the bridge excitation energy is much larger than the D and A excitation energies and (2) the one-electron coupling operator dominates the propagation mechanism.[22, 23] These early theoretical and experimental studies, and later seminal studies of Scholes, Harriman, Albinsonn, Speiser, and Baldo, established a semi-quantitative linkage between bridge-mediated electron-transfer and Dexter energy-transfer reactions.[4, 15, 22, 24-27]

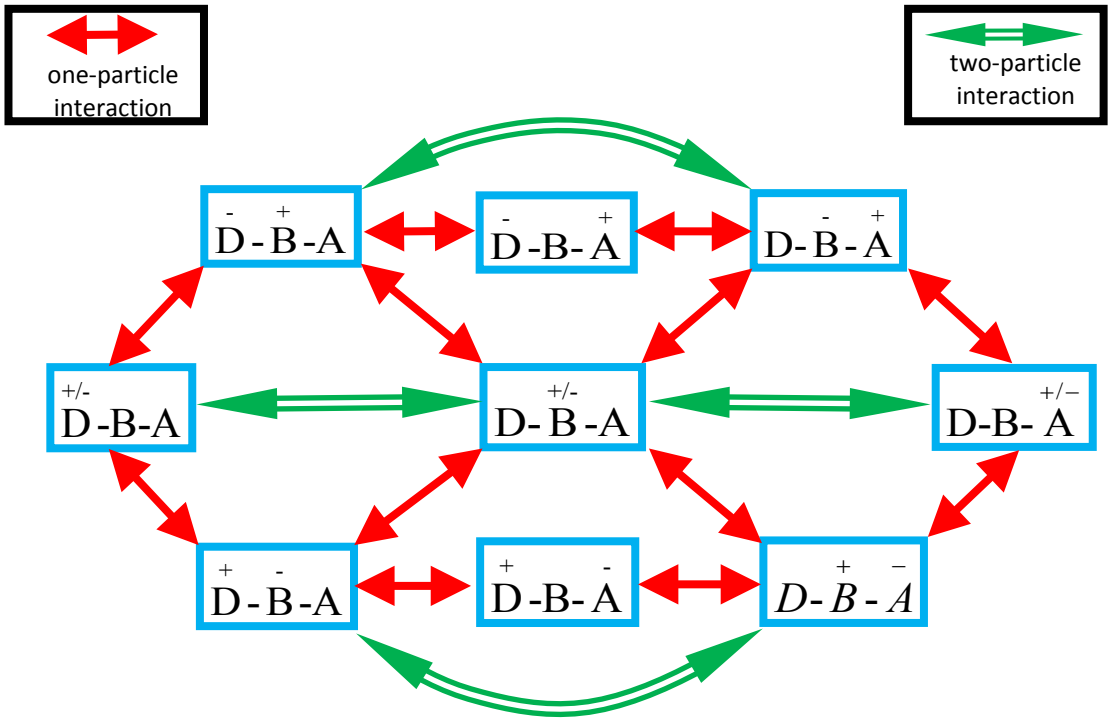

Figure 2. Schematic summary of the kinds of interaction that cause Dexter energy transfer in a bridged system from D*BA to DBA*. The action of the one-particle Hamiltonian operator on an excitonic state can propagate either an electron or a hole but not both. The action of a two-particle interaction Hamiltonian operator on an excitonic state simultaneously propagates an electron and a hole. In our pathway analysis, these interactions are computed as couplings between initial and final diabatic states of the D, B, and A species, obtained using the constrained DFT method.

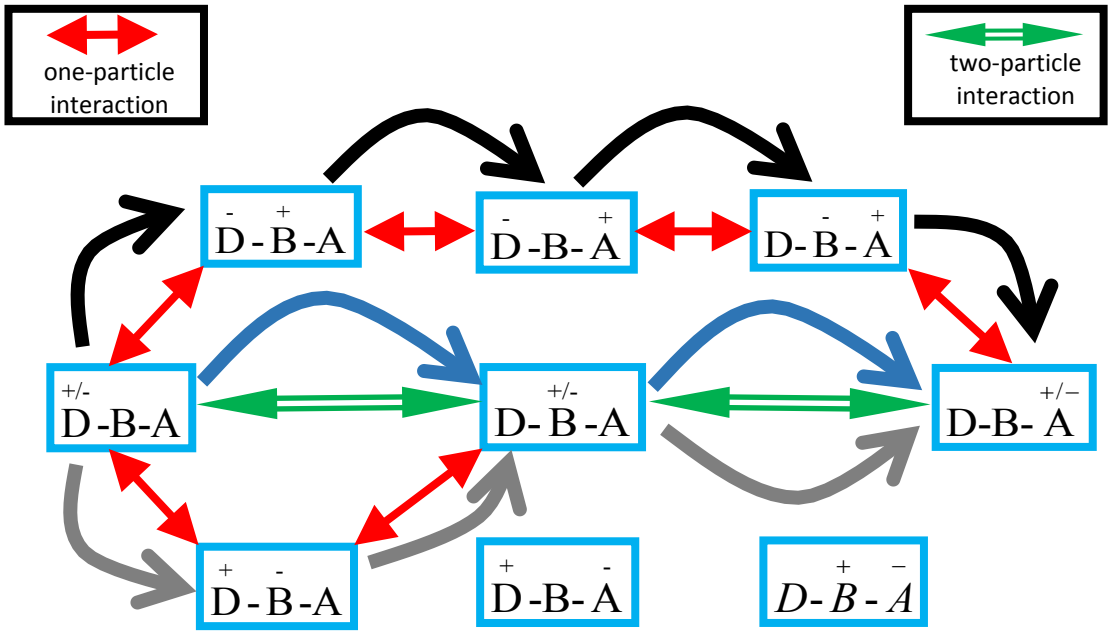

Figure 3. Schematic representation of Dexter coupling pathways in a simple DBA system. One sided arrows represent single steps within a Dexter pathway from D*BA to DBA*. The black one-sided arrows demark a four-step pathway with a DA charge transfer exciton intermediate (D^{-} B A^{+}) mediated solely by one-particle interactions. The blue one sided arrows indicate a two-step pathway with a bridge exciton intermediate (D $B^{+/-}$ A) mediated solely by two-particle interactions. The gray one sided arrows denote a three-step pathway with a bridge exciton intermediate (D $B^{+/-}$ A = DB*A) mediated by one particle interactions (first two steps) and a two-particle interaction (last step).

2. Early links between bridge-mediated Dexter energy transfer and electron transfer

The Dexter coupling approximation of Closs et al. is:[22, 23]

$$H_{DA}^{Dexter} \propto V^{e} \times V^{h}/\Delta E_{CT} \quad (3)$$

The electron- and hole-mediated superexchange interactions (defined as V^{e} and V^{h}, respectively) are one-electron transfer couplings. This approximation captures charge-transfer virtual states, neglecting bridge exciton virtual states and two-electron (Coulomb) mediated interactions. The values of V_{DA}^{e} and V_{DA}^{h} are the empirical electron- and hole-mediated superexchange interactions, and ΔE_{CT} is the average energy gap between the $D^{*}BA$ excited state and the charge-transfer states, $D^{+}BA^{-}$ and $D^{-}BA^{+}$. This formulation was validated successfully in experiments that

compared electron and energy transfer rates in rigid donor-bridge-acceptor structures with large B→B* excitation energy gaps.

2.1 Coupling pathways for electron transfer

Before addressing Dexter couplings and their dependence on bridge structure, we revisit the simpler case of electron or hole transfer though a single linear pathway and through two parallel paths.

2.1.1 Linear DBA Pathways

Assuming only nearest-neighbor interactions between sites, the lowest-order contribution to the bridge-mediated electron (hole) transfer coupling in the linear chain indicated in Figure 4 is $V_{DB}^{e(h)} V_{BA}^{e(h)}/\Delta E^{e(h)}$. $\Delta E^{e(h)}$ is the energy gap between the tunneling energy (for electron or hole transfer) and the mediating bridge state. The D and A state energies are assumed to be equal at the ET transition state.

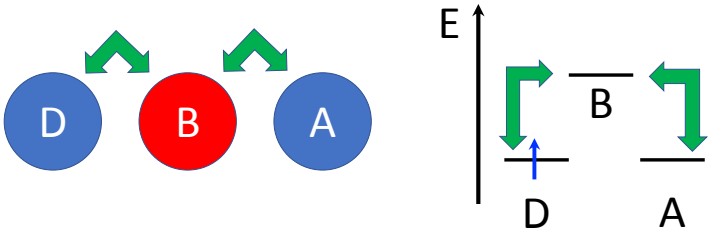

Figure 4. Schematic representation of a bridge-mediated donor acceptor interaction in a linear DBA chain. The lowest order superexchange coupling is $V_{DB}V_{BA}/\Delta E$ where V_{DB} and V_{BA} are the one-electron couplings between the D-B and B-A orbitals, respectively.

2.1.2 Parallel DBA Pathways

In the case of two parallel coupling routes with the same coupling interaction from D to the upper (U) and lower (L) bridge orbitals (Figure 5), the coupling is twice as strong as the interaction for the linear chain of Figure 4.[28] This doubling is expected when direct through-space DA interactions are weaker than the through-bond interactions, and when the value of V_{DB} and V_{BA} are equal in the two systems.

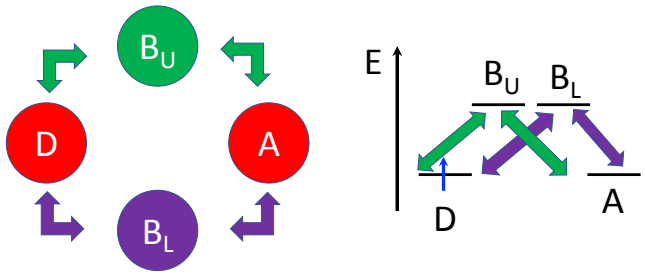

Figure 5. Schematic representation of a bridge with two equivalent parallel coupling pathways. The lowest-order contribution to the bridge-mediated superexchange coupling is $2V_{DB}V_{BA}/\Delta E$, where V_{DB} is the donor-bridge one-electron coupling, V_{BA} is the bridge-acceptor one-electron coupling and ΔE is the tunneling energy gap at the transition state for electron transfer. This enhanced coupling produce an electron or hole transfer rate that is four-times the rate in the linear bridge, since the golden rule rate is proportional to the squared coupling.

Recent studies also probed (theoretically) the effective coupling for two-electron transfer from D$^{=}$A to DA$^{=}$, indicated in Figure 6. The lowest order superexchange pathway for two-electron transfer generated by the one electron operator has the strength $-\frac{2V^4}{\Delta(\epsilon_B+\Delta)^2}-\frac{-4V^4}{2\epsilon_B(\epsilon_B+\Delta)^2}$ (see Figure 6 for definition of the symbols).[29] Two-electron superexchange interactions were not considered as they are assumed much weaker (proportional to squares of orbital overlaps rather than terms linear in overlaps).

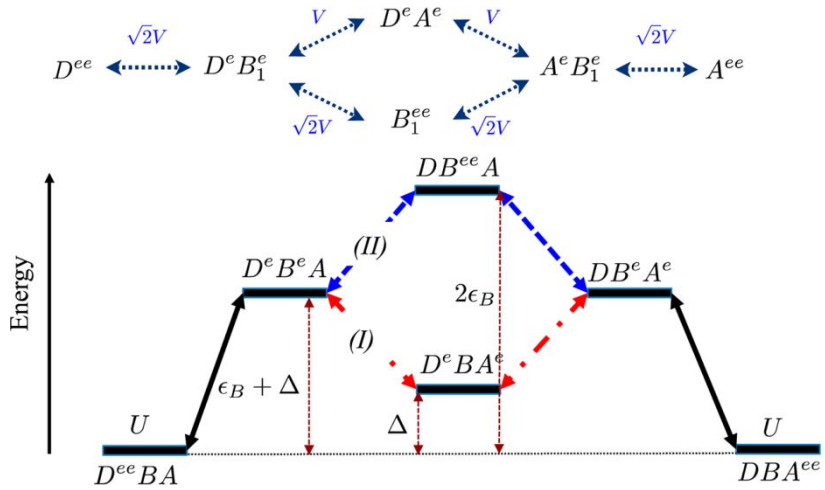

Figure 6. Schematic representation of a linear two-electron transfer pathway. The two-electron nature of the transition creates interferences between pathways with a doubly reduced bridge virtual state and a D->A charge transfer intermediate state. In this figure, *e* represents the positions of the mobile electrons (D^{ee} represents the doubly reduce donor, D^{e} represents the singly reduced donor, and *D* represents the fully oxidized donor, and analogous notation is used for B and A).

2.2 Dexter Coupling Pathways

What are the structure-function relationships that govern the Dexter mechanism? Figure 7 shows the qualitative energy landscape that governs bridge-mediated Dexter energy transfer. Here, d and d*, b and b*, and a and a* denote HOMOs and LUMOs of the donor, bridge and acceptor fragments, respectively.

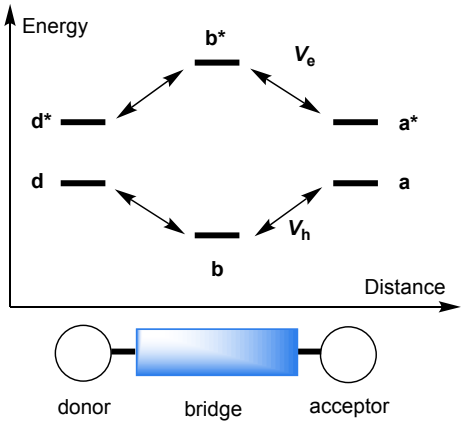

Figure 7. Electronic orbital landscape for Dexter coupling through-bond. V_h and V_e denote one-particle (electron and hole, respectively) Hamiltonian matrix elements between the fragment HOMOs and LUMOs, respectively. These electronic couplings produce bridge-mixed HOMOs and LUMOs that are donor centered ($|D\rangle \approx |d\rangle + |\delta_D^{br}\rangle$ and $|D^*\rangle \approx |d^*\rangle + |\delta_{D^*}^{br}\rangle$, respectively) and acceptor-centered ($|A\rangle \approx |a\rangle + |\delta_A^{br}\rangle$ and $|A^*\rangle \approx |a^*\rangle +$ $|\delta^{br}\rangle$

The simplest orbital description of a triplet donor exciton places a hole in the $|d\rangle$ orbital and an electron in the $|d^*\rangle$ orbital ($D^{+/-}$ configuration). The exciton can shift to the acceptor, producing a hole in $|a\rangle$, electron in $|a^*\rangle$ ($A^{+/-}$ configuration). The donor-acceptor charge-transfer (DA/CT) exciton intermediate states (D^+BA^- and D^-BA^+) define the one-particle contribution that was emphasized in early studies of Closs et al., and more recently in the analysis of Scholes and co-workers.[26, 30] To the best of our knowledge, the bridge exciton (BE) term was not explored in detail prior to our recent study.[3, 21] The BE term arises from bridge exciton virtual intermediates (DB*A). As such, the full Dexter coupling may be partitioned into three terms:

$$V_{triplet} \approx 2 \times \frac{V^e \times V^h}{\Delta E_{CT}} + BE - \left(DA \middle| D^* A^*\right) \quad (4)$$

The third term on the right side of Eq. 4 is the direct two-particle exchange coupling

$$(DA \,|\, D^* A^*) = \iint d^3r_1 d^3r_2 \phi_D(r_1)\phi_D(r_1) r_{12}^{-1} \phi_{D^*}(r_2)\phi_{A^*}(r_2) \quad (5)$$

Hartree-Fock single configuration interaction analysis and pathway analysis found that the BE contribution can be larger than the CT/DA contributions for long bridges or for bridges with low excitation energies.[3, 21] The contributions that arise from bridge exciton interactions can soften the approximately exponential distance decay of Dexter coupling.[21]

In summary, either the CT or BE contributions may dominate the Dexter coupling, depending on the molecular structure.[3, 21] These findings are based on a CIS formalism, where the one and two-electron interactions (beyond Hartree-Fock) are separated in the Hamiltonian. In the analysis below, we will use constrained DFT (CDFT) methods.

3. Assessing Dexter pathway interferences in non-covalent assemblies

Figure 8 shows three virtual states that contribute to exciton migration through a DBA system: the bridge exciton states (DB*A = $DB^{+/-}A$), the DB and BA electron/hole transfer states (e.g., D^+B^-A/ D^-B^+A), and the DA charge transfer (CT) exciton states (D^+BA^-/ D^-BA^+).

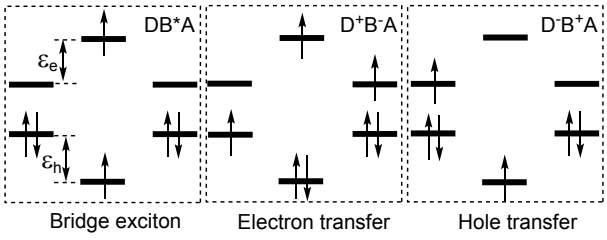

Figure 8. Electronic configurations of bridge exciton and charge transfer (electron and hole)

We next explore Dexter coupling and transport in model van der Waals structures, using naphthalene donors and acceptors with single and double ethylene bridges. The aim of these studies is to explore the quantum interference effects among parallel pathways.

All of the diabatic states related to Dexter energy transfer are constructed directly using constrained density functional theory (CDFT),[31-33] which is implemented in the QCHEM 4.4 quantum chemistry package.[34] In all the CDFT calculations, charge and spin density constraints on

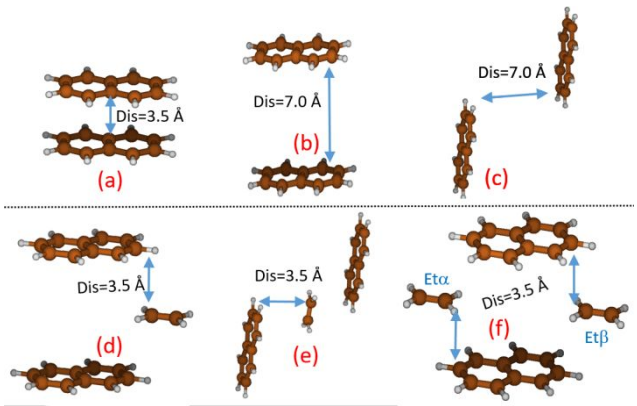

Figure 9. The geometry structures of the investigated molecular systems containing naphthalene (Nap) and ethylene (Et): (a) Sandwich Nap-Nap dimer with layer with 3.5 Å distance; (b) Sandwich Nap-Nap dimer with 7.0 Å distance; (c) Zigzag Nap-Nap dimer with 7.0 Å distance; (d) Sandwich Nap-Et-Nap complex; (e) Zigzag Nap-Et-Nap complex; (f) Sandwich-Nap-Et_U/Et_L-Nap complex.

each fragment (D/B/A) are enforced, and the lowest energy state subject to the density constraint is computed. With the Kohn-Sham wave function, the configuration interaction with constrained DFT method (CDFT-CI) is used to calculated the diabatic couplings[32], where the one- and two-electron matrix elements are reformed using the KS orbitals.[32] The accompanying DFT calculations were performed with PBE functionals[35] and the 6-31+G(d) basis set.[36] The Dexter coupling in stacked naphthalene-naphthalene dimers was computed and compared with the result from the fragment spin difference (FSD) method,[37] and the excellent performance confirmed the validity of the CDFT-CI approach on the current issues. (See Figure S3 of the SI).

Here, we examine Dexter energy transfer in the deep tunneling regime (i.e., there is a very large energy gap between the naphthalene and ethylene excitation energies), and the donor-acceptor coupling is computed using a Green's function approach.[3, 38]

We define the donor-bridge one-particle electron and hole interactions in the CDFT methodology, for example, as:

$$V_{DB}^{e} = \left\langle D^{+/-}BA \middle| \hat{H}^{KS} \middle| D^{+}B^{-}A \right\rangle \quad \text{(6a)}$$

$$V_{DB}^{h} = \left\langle D^{+/-}BA \middle| \hat{H}^{KS} \middle| D^{-}B^{+}A \right\rangle \quad \text{(6b)}$$

All other one-particle interactions are constructed by analogy with these terms.

We define the two-particle interactions among diabatic states in the CDFT methodology, for example, as:

$$V_{D^{+}B^{-}A,DB^{-}A^{+}}^{eh} = \left\langle D^{+}B^{-}A \middle| \hat{H}^{KS} \middle| DB^{-}A^{+} \right\rangle \quad (7)$$

All other two-particle interactions are constructed by analogy with these terms. As a special case, for the two-particle interaction between the initial and final states for Dexter transfer, we name the direct coupling two-particle interaction V_{direct}:

$$V_{direct} = V_{D^{*}BA,DBA^{*}}^{eh} = \left\langle D^{*}BA \middle| \hat{H}^{KS} \middle| DBA^{*} \right\rangle \quad (8)$$

The geometries of the molecular structures are shown in Figure 9. We begin with three naphthalene dimers, two in a "sandwich" structure, and one in a "zigzag" structure (see Figure 9 a-c). Then, we introduce one ethylene bridging molecule between the napthalenes to produce D-B-A structures with a stacked or an offset architecture (Figure 8d, e). Finally we introduce two ethylene bridging molecules to produce a D-B_U/B_L-A structure with two parallel pathways (Figure

8f).

3.1 Pathway interference in the D-A structure

In the D-A structure, Dexter coupling is limited to one-particle (1p) pathways involving the charge transfer (CT) exciton states (D^+A^-/ D^-A^+) and two-particle (2p) pathway involving the two-particle exchange coupling. All of the coupling terms that contribute to the 1p pathways between the nearest-neighbor states are coupled by one-particle interactions. The 2p pathways have couplings that arise from the two-particle interactions. We calculated all the state energies and couplings among the associated diabatic states of the three pathways, and the results are shown in the SI. With these computed interaction elements, the effective donor-acceptor couplings were computed using a Green's function approach (see Table 1).

The Dexter pathways in the Nap-Nap dimer at 3.5 Å (see Figure 9a) are. Because of the short Nap-Nap distance and the mirror symmetry, both the one-electron and two-electron interactions are larger than 0.1 eV, although the one-electron coupling is larger. Examining the one-electron terms in eq. 4:

:

$$V_{1e}^{eff} = -2\frac{V_{DA}^{h} \times V_{D^*A^*}^{e}}{\Delta E_{CT}} = -\frac{0.67 \times 0.60}{2.3} eV = -0.35\ eV \qquad (9)$$

The direct two-particle coupling interaction (V_{direct}) is -0.14 eV, which is somewhat less than the one-electron coupling.

The magnitudes of the couplings from the one-electron pathways and direct two-particle interaction, V_{1e}^{eff} and V_{direct} are also of the same order in the other two Nap-Nap dimers at larger distances (Figure 8b and 8c). V_{direct} can be even larger than V_{1e}, indicating that the direct coupling mechanism may not generally be ignored. Although the single one-electron interactions is always larger than the two-electron interactions, the V_{1e} Dexter coupling is the product of two one-electron interactions divided by ΔE_{CT}. As a result, the calculated V_{1e}^{eff} Dexter coupling from eq. 9 is the same order of magnitude as V_{direct}.

The 7 Å distance (Figure 8 a,b), the couplings decrease substantially. The electron transfer coupling is reduced by a factor of 10^3, while V_{1e}^{eff} for Dexter transfer is decreased by 10^6. When we slide the Nap-Nap dimer into a zigzag geometry, the coupling decrease because of the weakened orbital overlap.

There is quantum interference between the two one-electron Dexter coupling pathways in the nap-nap structure (D*A -> D+A- -> DA* and D*A -> D-A+ -> DA*). The difference between V_{1e}^{eff} and V_{br} presents the quantum interferences (see eqs 6 and 7). The coupling between the two CT states enhances the bridge-mediated coupling by 0.06 eV. We can understand this constructive interference from two different perspectives.

When the coupling $V_{D^+A^-/D^-A^+}^{ee}$ is non-zero, two adiabatic mixed CT states are generated (from a mixture of D^-A^+ and D^+A^- states). The symmetric combination will couple the donor and acceptor states effectively, while the antisymmetric combination gives zero coupling because of destructive interference. Whether the final coupling V_{br} is enhanced or decreased depends on the energy of the symmetric combination state, which is determined by the sign of the interstate coupling. The influence of $V_{D\text{-}A+/D+A^-}$ on the coupling is:

$$V_{br}^{eff} = -2\frac{V_{DA}^{h} \times V_{D^*A^*}^{e}}{\Delta E_{CT} + V_{D^+A^-/D^-A^+}} \qquad (10)$$

for the symmetric dimer.

The interstate coupling also activates two more pathways: D*A →D^-A^+→D^+A^-→DA* and D*A →D^+A^-→D^-A^+→DA*. Adding the coupling of the new pathways to V_{1e}, the full bridge-mediated coupling is:

$$V_{br}^{eff} = -2\frac{V_{DA}^{h} \times V_{D^*A^*}^{e}}{\Delta E_{CT}} + 2\frac{V_{DA}^{h} \times V_{D^*A^*}^{e} \times V_{D^+A^-/D^-A^+}^{eh}}{\Delta E_{CT}\Delta E_{CT}}$$

$$= -2\frac{V_{DA}^{h} \times V_{D^*A^*}^{e}}{\Delta E_{CT}^{2}}(\Delta E_{CT} - V_{D^+A^-/D^-A^+}) = -2\frac{V_{DA}^{hole} \times V_{D^*A^*}^{el}}{\Delta E_{CT} + V_{D^+A^-/D^-A^+}}\ (1 - \frac{V_{D^+A^-/D^-A^+}^{2}}{\Delta E_{CT}^{2}}) \qquad (11)$$

When $V_{D\text{-}A+/D+A^-} << \Delta E_{CT}$, the effective couplings in eqs (7) and (8) will be nearly the same. In this case, the sign of the additional pathways determines the nature of the interference (constructive/destructive).

Eq. 10 is exact but difficult to use for complicated systems. Eq. 11 is linked directly to the coupling pathways and is more convenient to assess interferences.

Table 1. Calculated couplings of the molecular systems shown in Figure 9: the direct coupling for electron transfer (V_{ET_d}); the bridge mediated coupling for electron transfer (V_{ET_br}); the direct coupling for hole transfer (V_{HT_d}); the bridge mediated coupling for hole transfer (V_{HT_br}); the sum of couplings for Dexter transfer from one electron bridge mediated pathways (V_{1e}^{eff}); the sum of couplings for Dexter transfer from bridge-mediated mechanism (V_{br}^{eff}); the direct coupling for Dexter transfer from two-particle interaction (V_{direct}); the total effective coupling for Dexter transfer (V_{total}^{eff}).

Structure	Sandwich Nap-Nap	Sandwich Nap-Nap	Zigzag Nap-Nap	Sandwich Nap-Et-Nap	Zigzag Nap-Et-Nap	Sandwich Nap-Et_UEt_LNap
	Fig. 8(a)	Fig. 8(b)	Fig. 8(c)	Fig. 8(d)	Fig. 8(e)	Fig. 8(f)

V_{ET_d}/eV	6.0×10^{-1}	4.6×10^{-3}	1.8×10^{-3}	3.4×10^{-3}	7.1×10^{-4}	-2.3×10^{-3}
V_{ET_br}/eV	-7.4×10^{-2}	1.8×10^{-9}	-5.8×10^{-10}	-2.1×10^{-3}	-1.9×10^{-3}	3.4×10^{-3}
V_{HT_d}/eV	6.7×10^{-1}	2.4×10^{-3}	3.5×10^{-4}	-4.5×10^{-3}	-3.4×10^{-4}	-7.0×10^{-3}
V_{HT_br}/eV	-6.8×10^{-2}	3.4×10^{-9}	-3.0×10^{-9}	-3.0×10^{-3}	-4.1×10^{-3}	-5.8×10^{-3}
V_{1e}^{eff}/eV	-3.5×10^{-1}	-6.9×10^{-6}	-3.4×10^{-7}	-6.0×10^{-6}	3.3×10^{-6}	-1.2×10^{-5}
V_{br}^{eff}/eV	-4.1×10^{-1}	-6.9×10^{-6}	-3.4×10^{-7}	-1.4×10^{-7}	3.1×10^{-5}	-6.0×10^{-5}
V_{direct}/eV	-1.4×10^{-1}	-1.1×10^{-5}	-5.6×10^{-8}	1.1×10^{-5}	5.4×10^{-6}	8.2×10^{-6}
V_{total}^{eff}/eV	-5.5×10^{-1}	-1.8×10^{-5}	-4.0×10^{-7}	1.1×10^{-5}	3.6×10^{-5}	-5.2×10^{-5}

3.2 Dexter coupling pathways in bridged systems

For bridge-mediated systems, such as D-B-A complexes, the CDFT analysis allows us to compute the one- and two-particle interactions needed to quantify the couplings indicated in Figure 2 and to derive coupling pathways as indicated in Figure 3.

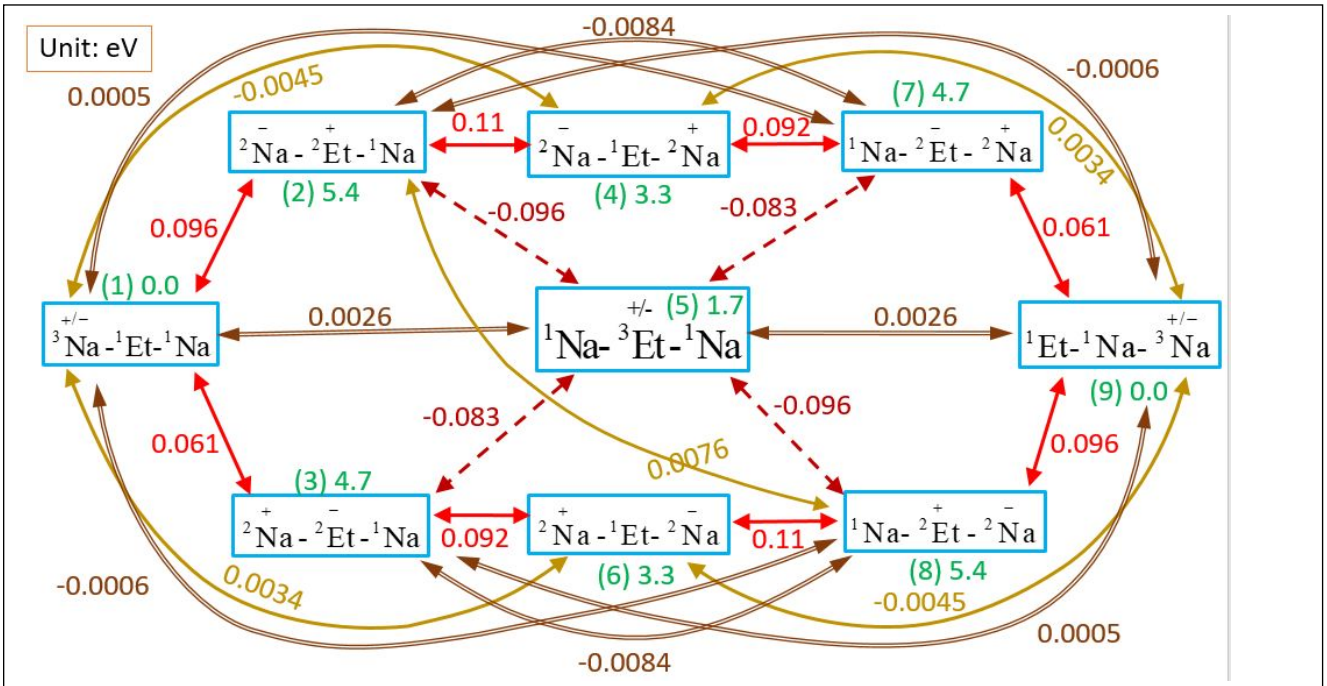

Figure 10. The state energies and couplings between related diabatic states for the sandwich-Nap-Et-Nap structure. Numbers in green indicate state energies, numbers near single lines indicate one-electron couplings, numbers near double lines indicate two-electron couplings.

We started with the Sandwich-Nap-Et-Nap in Figure 9d, and the essential pathways for the final effective Dexter coupling are shown in Figure 10. Among the six one-electron bridge-mediated pathways shown in Figure 10, four arise from the BE contribution, and the others arise from CT contributions. From the interactions in Figure 10, we find that the effective coupling from the two CT pathways is -1.4×10^{-6} eV, while the effective coupling from the four BE pathways is -4.6×10^{-6} eV. The sum of the pathways provides the total effective one-electron pathway coupling, V_{1e}^{eff}. The larger magnitude BE contribution arises because the BE states have lower energies than the CT states, and the number of BE pathways is twice as large as the number of CT pathways.

In D-A systems, we know that direct Dexter coupling from two-particle interactions is comparable in magnitude to the effective one-electron coupling. In D-B-A systems, the two-particle operator introduces more mediating states than does the pure one-particle operator, including mixed 1e/2e pathways. Although the pure 2e coupling term is usually smaller than the 1e coupling term, 2e pathways and mixed 1e/2e pathways can have fewer steps than pure 1e pathways, which may produce couplings comparable to or stronger than the pathways based only on 1e interactions. As an example, the pure 2e pathway (Figure 10) linking states 1, 5, and 9 has a pathway coupling of -4.0×10^{-6} eV, which is very close to the pure V_{1e} coupling value.

The interactions represented by dark yellow lines in Figure 8 are dominated by the interaction between the two naphthalene molecules through space, while the bridging ethylene makes little contribution. If we remove all these space coupling pathways denoted in the figure with dark yellow lines, then the effective bridge-mediated coupling grow to -1.2×10^{-5} eV. If we retain just the dark yellow terms, the bridge-mediated coupling is 9.3×10^{-6} eV. These two values are similar in magnitude to each other, but have the opposite signs, so they interfere destructively. This interference explains the small overall bridge-mediated coupling V_{br}^{eff} in the structure. In the next structure studied, we weaken the naphthalene-napthalene interaction through space.

In the zigzag-Nap-Et-Nap system with offset naphthalene units, the orbital overlap between the naphthalene molecules is much smaller, and the space interaction between them is therefore much weaker. The pathway map is shown in Figure 11. In contrast to the sandwich-geometry Nap-Et-Nap structure, where the bridge-mediated ET/HT couplings and through-space couplings are similar in magnitude, the zigzag structure has much smaller Nap-Nap through-space couplings.

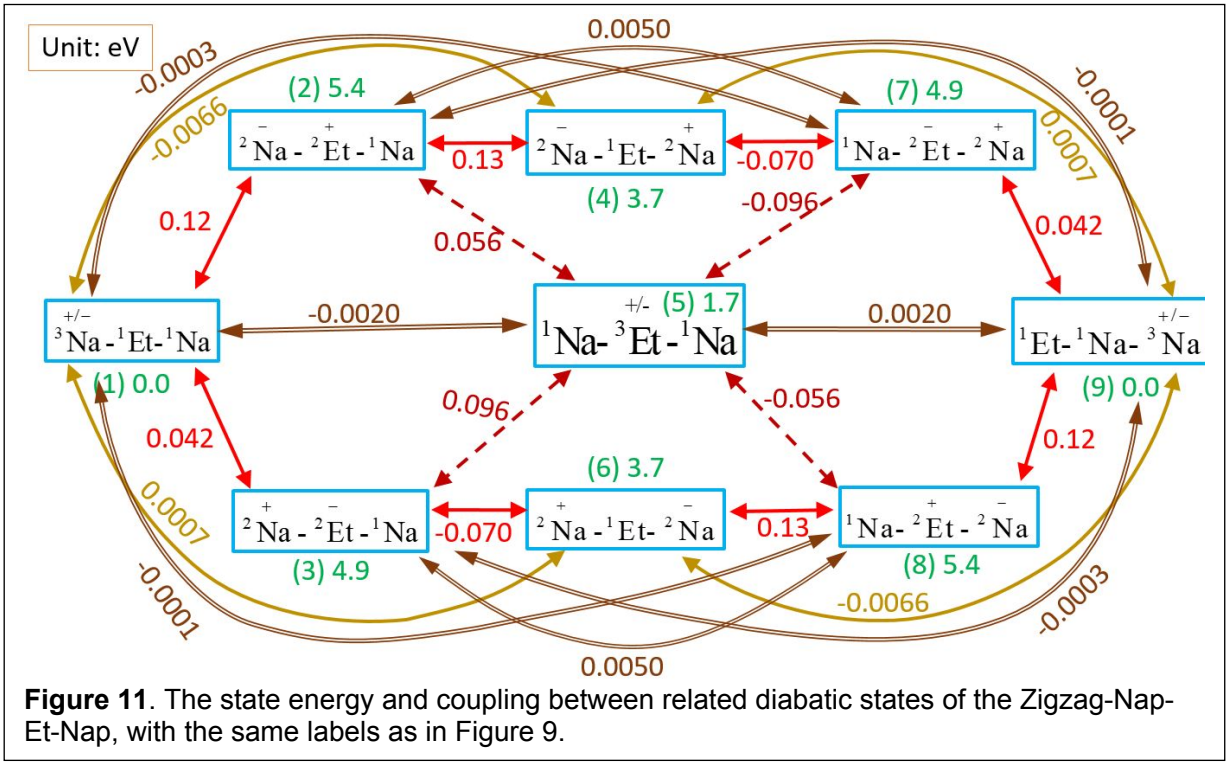

Figure 11. The state energy and coupling between related diabatic states of the Zigzag-Nap-Et-Nap, with the same labels as in Figure 9.

The effective 1e coupling (V_{1e}^{eff}) in the zigzag Nap-Et-Nap geometry is 3.3×10^{-6} eV, which is slightly smaller than the value in the sandwich Nap-Et-Nap structure. However, the overall bridge-mediated coupling (V_{br}) is 3.1×10^{-5} eV, much larger than the value in the sandwich-Nap-Et-Nap structure. The difference arises from the dark yellow through-space interaction pathways indicated in Figure 9. The couplings along these pathways are smaller, and more importantly, have the same sign as the other bridge-mediated pathways. As a consequence, destructive interference of bridge-mediated and through-space interaction pathways in the Nap-Et-Nap sandwich structure changes to a

constructive interference effect in the zigzag-Nap-Et-Nap structure, enhancing the bridge-mediated coupling, V_{br}^{eff}.

3.3 Dexter Pathways in Parallel-Bridge-Mediated Systems.

We now examine the case of two parallel ethylene-mediated system shown in Figure 9f. For single electron or hole transfer, the bridge-mediated superexchange interaction is expected to be doubled for two equivalent bridges compared to just one, which is confirmed by the V_{HT_br} and V_{HT_br} values in Table 1. For the Dexter couplings, the number of one-electron pathways grow by a factor of four, since each transiting electron and each hole may choose the upper (U) or the lower (L) superexchange pathway ($2 \times 2 = 4$). Note, however, that the superexchange pathways have the two different energies for BE virtual states, depending upon whether or not the electron and hole reside on the same of different ethylene molecules. As a result, there are 24 unique pathways generated by the one-electron operator in the structures with two ethylene bridges (see Figure S2 of SI), rather than just 6 one-electron operator generated pathways in the case of one ethylene bridge. (See SI for further discussion). If the coupling mediated by each pathway were identical, then the sum of the coupling strengths V_{1e}^{eff} would be increased by a factor of 4.

A factor of 2 instead of a factor of 4 arises for V_{1e}^{eff} for the one vs. two ethylene sandwich bridge structures. This is because the 24 one-particle Dexter pathways have a wide range of excited state energies. The BE energies are also very different when the electron and hole reside on the same vs. different ethylene molecules of the bridge (i.e., 1.7 eV vs. 7.9 eV, respectively). If we consider only the lower energy BE pathways, then the number of sandwich-Nap-Et-Nap pathways is 4, while the number of sandwich-Nap-Et_U/Et_L-Nap is 8, which explains the factor of 2 coupling enhancement for the double ethylene structure. It will be interesting to explore how the enhancement factor may be manipulated by further modifying the bridging structure.

For the sandwich-Nap-Et-Nap structure, coupling that arises from the through-space interaction between the two naphthalenes (represented by dark yellow lines) is close to the effective bridge-mediated coupling (but with opposite sign), leading to the very small overall bridge-mediated coupling. This naphthalene-napthalene through-space interaction will change little as ethylene bridges are added, while the bridge-mediated coupling is expected to grow with the number of

parallel coupling pathways. As a result, the sum of the through-space (one particle) and the effective bridge-mediated coupling increases from 1×10^{-7} eV to 6×10^{-5} eV (as we change from a one ethylene to a two ethylene bridge), and the total effective Dexter coupling increases from 1×10^{-5} to 5×10^{-5} eV.

The effective 1e bridge-mediated pathway coupling (V_{1e}^{eff}) is just 20% of the entire bridge-mediated coupling V_{br}^{eff}, so the one-particle, two-particle and mixed one-particle/two-particle pathways are all essential for the final effective coupling in this structure. As such, the nature of Dexter pathway interferences is much richer and more varied than in the case of single electron superexchange.

4. Summary and Conclusions.

We have studied the dependence of the bridge-mediated coupling in Dexter energy transfer systems with the architectures: D-A, D-B-A and D-B_UB_L-A using constrained DFT methods. The differences nature of the Dexter coupling pathway interferences were explored and contrasted with the results for single electron or hole transfer.

We find that the two particle coupling interactions establish effective coupling pathways for some of the Dexter energy transfer systems described here. Although the two-electron couplings are smaller than the one-electron coupling, they can produce pathways with fewer steps, and can dominate. Mixed one- and two-electron transfer pathways also contribute significantly to the bridge-mediated couplings. For electron transfer, the shortest and strongest pathways are usually a sequence of one-electron or one-hole steps.

Simple pathway arguments about quantum interference effects based on pathway counting for the Dexter mechanism are not useful for predicting the strength of parallel pathway interference effects because the energies of the virtual states depend strongly on the physical position of the electron and the hole states. In the case of the noncovalent ethylene bridged systems studied here, equivalent parallel pathway produce constructive interference effect of a factor of two, similar to the case in single electron transfer. The reason that there is not a larger combinatorial factor is that many of the virtual states are sufficiently off of resonance that they make little net contribution to the bridge-mediated coupling. Further studies of bridge-mediated coupling effects in covalent and non-covalent systems should reveal whether systems could be designed that capture the stronger pathway enhancement that might be expected by state counting. It is also interesting to reflect on the possibility of developing phosphorescence probes that could be

sensitive the molecular structure of the material intervening between the absorbing and phosphorescent donor and acceptor chromophores.

Acknowledgments

This research was supported by the U.S. Department of Energy, Office of Science, Office of Basic Energy Sciences, under Award DE-SC0019400.

Conflicts of Interest

The authors declare not conflicts of interest.

References

1. R. E. Blankenship, *Molecular Mechanisms of Photosynthesis*, Wiley-Blackwell, 2nd edn., 2014.

2. V. May and O. Kühn, *Charge and Energy Transfer Dynamics in Molecular Systems*, Wiley, Weinheim, 3rd edn., 2011.

3. S. S. Skourtis, C. R. Liu, P. Antoniou, A. M. Virshup and D. N. Beratan, *Proc. Natl. Acad. Sci. U.S.A.*, 2016, **113**, 8115-8120.

4. S. Speiser, *Chem. Rev.*, 1996, **96**, 1953-1976.

5. T. Förster, *Ann Phys-Berlin*, 1948, **2**, 55-75.

6. D. L. Dexter, *J. Chem. Phys.*, 1953, **21**, 836-850.

7. A. Ito, D. J. Stewart, Z. Fang, M. K. Brennaman and T. J. Meyer, *Proc. Natl. Acad. Sci. U.S.A.*, 2012, **109**, 15132-15135.

8. F. Schmitt, J. Freudenreich, N. P. E. Barry, L. Juillerat-Jeanneret, G. Suss-Fink and B. Therrien, *J. Am. Chem. Soc.*, 2012, **134**, 754-757.

9. S. Omagari, T. Nakanishi, Y. Kitagawa, T. Seki, K. Fushimi, H. Ito, A. Meijerink and Y. Hasegawa, *Sci. Rep.*, 2016, **6**, 37008.

10. X. Li, Z. Y. Huang, R. Zavala and M. L. Tang, *J Phys Chem Lett*, 2016, **7**, 1955-1959.

11. C. Mongin, S. Garakyaraghi, N. Razgoniaeva, M. Zamkov and F. N. Castellano, *Science*, 2016, **351**, 369-372.

12. M. Tabachnyk, B. Ehrler, S. Gelinas, M. L. Bohm, B. J. Walker, K. P. Musselman, N. C. Greenham, R. H. Friend and A. Rao, *Nat. Mater.*, 2014, **13**, 1033-1038.

13. C. A. Kent, D. Liu, T. J. Meyer and W. Lin, *J. Am. Chem. Soc.*, 2012, **134**, 3991-3994.

14. M. C. So, G. P. Wiederrecht, J. E. Mondloch, J. T. Hupp and O. K. Farha, *Chem. Commun.*, 2015, **51**, 3501-3510.

15. R. J. Cogdell and H. A. Frank, *Biochim. Biophys. Acta*, 1987, **895**, 63-79.

16. Z. Y. Huang, P. Xia, N. Megerdich, D. A. Fishman, V. I. Vullev and M. L. Tang, *Acs Photonics*, 2018, **5**, 3089-3096.

17. Z. Chen, H. Y. Hsu, M. Arca and K. S. Schanze, *J. Phys. Chem. B*, 2015, **119**, 7198-7209.

18. X. Li, M. Bird, G. Mauro, S. Asaoka, A. R. Cook, H. C. Chen and J. R. Miller, *J. Phys. Chem. B*, 2015, **119**, 7210-7218.

19. K. Ema, M. Inomata, Y. Kato and H. Kunugita, *Phys. Rev. Lett.*, 2008, **100**, 257401.

20. J. M. Ho, E. Kish, D. D. Mendez-Hernandez, K. WongCarter, S. Pillai, G. Kodis, J. Niklas, O. G. Poluektov, D. Gust, T. A. Moore, A. L. Moore, V. S. Batista and B. Robert, *Proc. Natl. Acad. Sci. U.S.A.*, 2017, **114**, E5513-E5521.

21. P. Antoniou, Ph.D. Thesis, University of Cyprus, 2017.

22. G. L. Closs, M. D. Johnson, J. R. Miller and P. Piotrowiak, *J. Am. Chem. Soc.*, 1989, **111**, 3751-3753.

23. G. L. Closs, P. Piotrowiak, J. M. Macinnis and G. R. Fleming, *J. Am. Chem. Soc.*, 1988, **110**, 2652-2653.

24. M. A. Baldo, D. F. O'Brien, Y. You, A. Shoustikov, S. Sibley, M. E. Thompson and S. R. Forrest, *Nature*, 1998, **395**, 151-154.

25. V. Grosshenny, A. Harriman, M. Hissler and R. Ziessel, *J. Chem. Soc., Faraday Trans.*, 1996, **92**, 2223-2238.

26. R. D. Harcourt, G. D. Scholes and K. P. Ghiggino, *J. Chem. Phys.*, 1994, **101**, 10521-10525.

27. G. D. Scholes, *Acs Nano*, 2008, **2**, 523-537.

28. D. N. Beratan and J. J. Hopfield, *J. Am. Chem. Soc.*, 1984, **106**, 1584-1594.

29. J. X. Lin, D. Balamurugan, P. Zhang, S. S. Skourtis and D. N. Beratan, *J. Phys. Chem. B*, 2015, **119**, 7589-7597.

30. G. D. Scholes and K. P. Ghiggino, *J. Chem. Phys.*, 1994, **101**, 1251-1261.

31. T. Van Voorhis, T. Kowalczyk, B. Kaduk, L. P. Wang, C. L. Cheng and Q. Wu, *Annu. Rev. Phys. Chem.*, 2010, **61**, 149-170.

32. Q. Wu and T. Van Voorhis, *J. Chem. Phys.*, 2006, **125**, 164105.

33. S. Yeganeh and T. Van Voorhis, *J. Phys. Chem. C*, 2010, **114**, 20756-20763.

34. Y. H. Shao, Z. T. Gan, E. Epifanovsky, A. T. B. Gilbert, M. Wormit, J. Kussmann, A. W. Lange, A. Behn, J. Deng, X. T. Feng, D. Ghosh, M. Goldey, P. R. Horn, L. D. Jacobson, I. Kaliman, R. Z. Khaliullin, T. Kus, A. Landau, J. Liu, E. I. Proynov, Y. M. Rhee, R. M. Richard, M. A. Rohrdanz, R. P. Steele, E. J. Sundstrom, H. L. Woodcock, P. M. Zimmerman, D. Zuev, B. Albrecht, E. Alguire, B. Austin, G. J. O. Beran, Y. A. Bernard, E. Berquist, K. Brandhorst, K. B. Bravaya, S. T. Brown, D. Casanova, C. M. Chang, Y. Q. Chen, S. H. Chien, K. D. Closser, D. L. Crittenden, M. Diedenhofen, R. A. DiStasio, H. Do, A. D. Dutoi, R. G. Edgar, S. Fatehi, L. Fusti-Molnar, A. Ghysels, A. Golubeva-Zadorozhnaya, J. Gomes, M. W. D. Hanson-Heine, P. H. P. Harbach, A. W. Hauser, E. G. Hohenstein, Z. C. Holden, T. C. Jagau, H. J. Ji, B. Kaduk, K. Khistyaev, J. Kim, J. Kim, R. A. King, P. Klunzinger, D. Kosenkov, T. Kowalczyk, C. M. Krauter, K. U. Lao, A. D. Laurent, K. V. Lawler, S. V. Levchenko, C. Y. Lin, F. Liu, E. Livshits, R. C. Lochan, A. Luenser, P. Manohar, S. F. Manzer, S. P. Mao, N. Mardirossian, A. V. Marenich, S. A. Maurer, N. J. Mayhall, E. Neuscamman, C. M. Oana, R. Olivares-Amaya, D. P. O'Neill, J. A. Parkhill, T. M. Perrine, R. Peverati, A. Prociuk, D. R. Rehn, E. Rosta, N. J. Russ, S. M. Sharada, S. Sharma, D. W. Small, A. Sodt, T. Stein, D. Stuck, Y. C. Su, A. J. W. Thom, T. Tsuchimochi, V. Vanovschi, L. Vogt, O. Vydrov, T. Wang, M. A. Watson, J. Wenzel, A. White, C. F. Williams, J. Yang, S. Yeganeh, S. R. Yost, Z. Q. You, I. Y. Zhang, X. Zhang, Y. Zhao, B. R. Brooks, G. K. L. Chan, D. M. Chipman, C. J. Cramer, W. A. Goddard, M. S. Gordon, W. J. Hehre, A. Klamt, H. F. Schaefer, M. W. Schmidt, C. D. Sherrill, D. G. Truhlar, A. Warshel, X. Xu, A. Aspuru-Guzik, R. Baer, A. T. Bell, N. A. Besley, J. D. Chai, A. Dreuw, B. D. Dunietz, T. R. Furlani, S. R. Gwaltney, C. P. Hsu, Y. S. Jung, J. Kong, D. S. Lambrecht, W. Z. Liang, C. Ochsenfeld, V. A. Rassolov, L. V. Slipchenko, J. E. Subotnik, T. Van Voorhis, J. M. Herbert, A. I. Krylov, P. M. W. Gill and M. Head-Gordon, *Mol. Phys.*, 2015, **113**, 184-215.

35. J. P. Perdew, K. Burke and M. Ernzerhof, *Phys. Rev. Lett.*, 1996, **77**, 3865-3868.

36. W. J. Hehre, R. Ditchfield. and J. A. Pople, *J. Chem. Phys.*, 1972, **56**, 2257-2261.

37. Z. Q. You and C. P. Hsu, *J. Chem. Phys.*, 2010, **133**.

38. S. S. Skourtis and D. N. Beratan, *Adv. Chem. Phys.*, 1999, **106**, 377-452.